A disordered rock-salt Li-excess cathode material with high capacity and substantial oxygen redox activity: $Li_{1.25}Nb_{0.25}Mn_{0.5}O_2$

Rui Wang [a], Xin Li [a,b], Lei Liu [a], Jinhyuk Lee [a], Dong-Hwa Seo [a], Shou-Hang Bo [a], Alexander Urban [a], Gerbrand Ceder [c,d,*]

[a] Department of Materials Science and Engineering, Massachusetts Institute of Technology, Cambridge, MA 02139, USA
[b] John A. Paulson School of Engineering and Applied Sciences, Harvard University, Cambridge, MA 02138, USA
[c] Department of Materials Science and Engineering, UC Berkeley, Berkeley, CA 94720, USA
[d] Materials Science Division, Lawrence Berkeley National Laboratory, Berkeley, CA 94720, USA

ARTICLE INFO

ABSTRACT

A disordered rocksalt Li-excess cathode material, $Li_{1.25}Nb_{0.25}Mn_{0.5}O_2$, was synthesized and investigated. It shows a large initial discharge capacity of 287 mAh g^{-1} in the first cycle, which is much higher than the theoretical capacity of 146 mAh g^{-1} based on the Mn^{3+}/Mn^{4+} redox reaction. In situ X-ray diffraction (XRD) demonstrates that the compound remains cation-disordered during the first cycle. Electron energy loss spectroscopy (EELS) suggests that Mn and O are likely to both be redox active, resulting in the large reversible capacity. Our results show that $Li_{1.25}Nb_{0.25}Mn_{0.5}O_2$ is a promising cathode material for high capacity Li-ion batteries and that reversible oxygen redox in the bulk may be a viable way forward to increase the energy density of lithium-ion batteries.

Published by Elsevier B.V.

1. Introduction

There is an important need to create electrode materials for energy storage with higher capacity than what is currently available. Commercial cathodes for Li-ion batteries are typically derived from a few basic structure types such as the layered $NaFeO_2$-type structure, spinels, and olivines. These structures have been exhaustively investigated with various compositions based on classic 3d-metal redox couples such as Co, Ni, Mn and Fe, and novel ideas to increase the capacity of electrode materials are needed. We demonstrate here a disordered rocksalt with high electrochemical capacity provided in large part by reversible oxygen redox in the solid state. We believe that this finding sets an important new direction for high capacity cathode design with reduced transition metal content.

Layered Li-excess cathode materials have attracted tremendous attention recently due to their large capacities [1]. Compared with traditional layered materials, Li-excess materials can deliver much higher capacities from 250 up to 300 mAh g^{-1} [2–4], which has been attributed to the additional charge compensation mechanism activated by Li-excess through either the oxidation of O^{2-} to O^- or the release of O_2 [5–8] followed by cation densification. More recently, the design space for Li-excess materials was broadened to rocksalts with partial

or complete cation disorder through the understanding that more than 10% Li-excess creates a percolation network of 0-TM channels through which Li can diffuse, despite the large degree of cation disorder. Such high capacity Li-excess disordered materials have recently been demonstrated in several chemical systems [9–13]. However, the excess Li needed to enhance Li diffusion reduces the number of sites available for the transition metal redox center, and the theoretical metal-redox capacity is further decreased by the need for a high-valent metal to compensate for the Li-excess. Hence, in order to achieve optimized electrochemical performance, the composition of a compound is to be designed as a delicate balance between Li-excess and metal redox capability [14].

Very recently, significant success was achieved with Nb-based disordered compounds [13]. In this manuscript, a cathode material with the composition of $Li_{1.25}Nb_{0.25}Mn_{0.5}O_2$ is, synthesized and investigated. The capacity of this compound is almost double to the theoretical capacity based on the Mn^{3+}/Mn^{4+} redox reaction. EELS results suggest that both Mn and O contribute to the charge transfer with the oxygen redox reaction occurring reversibly in the first cycle. These results show the possibility to design new disordered rocksalt Li-excess materials with additional capacity provided by the oxygen redox reaction.

2. Experimental

$Li_{1.25}Nb_{0.25}Mn_{0.5}O_2$ (LNMO) was prepared by a solid state reaction. Li_2CO_3, Mn_2O_3, and Nb_2O_5 were mixed in a Retsch PM200 planetary

ball mill for 5 h and then pressed into a pellet. The pellet was sintered at 1000 °C for 12 h under argon gas flow.

The LNMO active material and carbon black were mixed by ball milling at 300 rpm for 4 h. The mixture was then manually mixed with polytetrafluoroethylene (PTFE) and rolled into thin film. The weight ratio of the LNMO active material, carbon black, and binder in the electrode is 70:20:10. Cells were assembled following earlier reports [9,14] and cycled on an Arbin battery tester using a current of 10 mA g^{-1} at room temperature or 55 °C.

EELS spectra were obtained on a JEOL 2010F equipped with a Gatan spectrometer, using parallel incident electron beam and a semi-collection angle of 5.3 mrad in TEM mode.

In situ XRD was taken on a Bruker D8 X-ray diffractometer equipped with a Mo source in a home-made in-situ electrochemical cell with Be window. The in-situ cell was charged galvanostatically using a current of 6.4 mA g^{-1} between 4.8 V and 1.5 V on Solartron 1287 with each XRD pattern scanned from 15° to 30° for 1 h.

3. Results and discussion

The sample obtained after initial firing and subsequent ball milling was characterized through XRD and SEM. Fig. 1a shows the XRD pattern of the material after ball milling with carbon black, and displays the characteristic peaks of a disordered rock-salt without any impurity phase. Refinement was carried out in the 2θ range of 30–85° using the Fm-3 m space group (#225). A random mixture of Li, Nb, and Mn in the 4b position (1/2, 1/2, 1/2) is assumed, and the O atom is placed on the 4a position (0, 0, 0). In the refinement, the composition of $Li_{1.25}Nb_{0.25}Mn_{0.5}O_2$ is fixed according to the target stoichiometry. Rietveld refinement using this structural model yields excellent agreement with the experimental observation (Rwp = 2.639, χ^2 = 1.520).
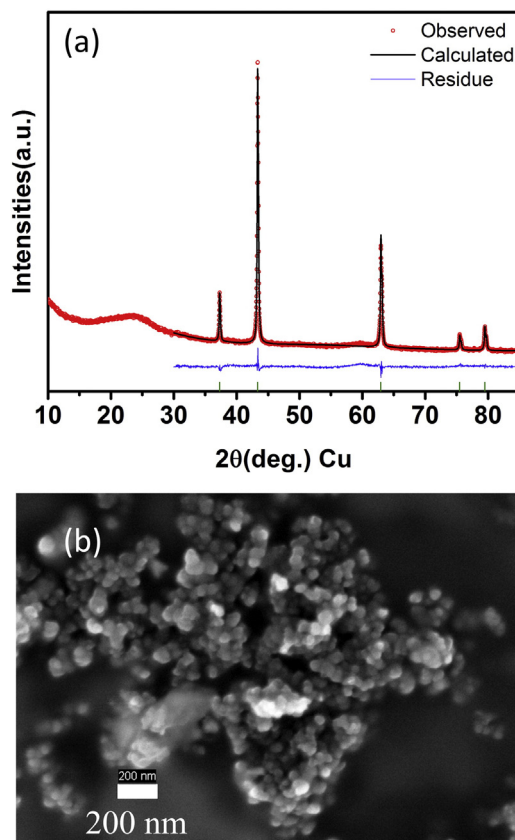

Fig. 1. (a) XRD pattern and (b) SEM picture of the $Li_{1.25}Nb_{0.25}Mn_{0.5}O_2$ material after ball milling with carbon black.

The lattice parameter is given as 4.1738 (1) Å. The SEM image in Fig. 1b shows that the particle size is slightly smaller than 100 nm.

The charge and discharge profiles of LNMO at 55 °C and room temperature are shown in Fig. 2a and b, respectively. Theoretically, LNMO can deliver a capacity of 146 mAh g^{-1} based on the Mn^{3+}/Mn^{4+} redox reaction, and 366 mAh g^{-1} based on the lithium content. The
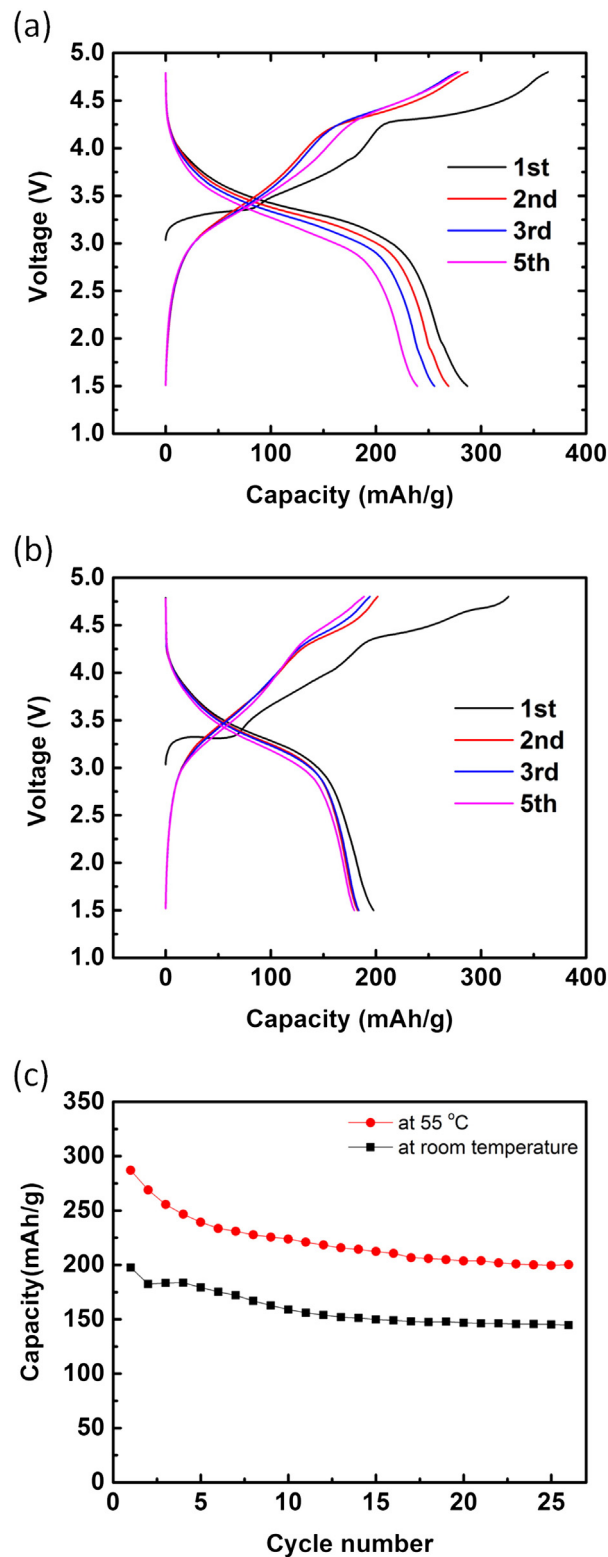

Fig. 2. Galvanostatic charge and discharge profiles at the 1st, 2nd, 3rd, and 5th cycles for $L_{1.25}Nb_{0.25}Mn_{0.5}O_2$ (a) at 55 °C and (b) room temperature. (c) Discharge capacity of $Li_{1.25}Nb_{0.25}Mn_{0.5}O_2$ cycled at 55 °C and room temperature versus cycle number.

initial charge capacities of both cells are higher than 300 mAh g^{-1}, with nearly all the lithium extracted out at 55 °C. In discharge, the cell cycled at 55 °C can deliver a capacity of 287 mAh g^{-1} and energy density of 909 Wh kg^{-1}, while the corresponding values at room temperature are 197 mAh g^{-1} and 627 Wh kg^{-1}. The difference may be caused by the increased lithium diffusivity at 55 °C. The voltage profile is somewhat different between the first and subsequent cycles which may come from some local structural changes (e.g. cation re-arrangement). The cycling performance presented in Fig. 2c shows that after 20 cycles the capacity converges to around 200 mAh g^{-1} for the sample at 55 °C, corresponding to an energy density of 601 Wh kg^{-1}.

It is especially encouraging to see such high initial charge and discharge capacities in LNMO at slightly elevated temperature. In order to understand the origin of the additional capacity beyond the theoretical value of 146 mAh g^{-1} expected from the Mn^{3+}/Mn^{4+} redox reaction, we performed in situ XRD and EELS measurements. Since our in situ cells have a relatively larger polarization, the in situ voltage profile is slightly different. The in situ XRD result in Fig. 3 shows the evolution of the characteristic (200) peak in the disordered rock-salt structure in the first cycle alongside the first charge and discharge profile. All the in situ XRD patterns in the first cycle are consistent with the disordered rock-salt structure. The lattice parameter evolution calculated from the in situ XRD data is also shown in Fig. 3. It indicates that upon initial charge the structure goes through a two-phase reaction, where the disappearing pristine phase keeps a constant lattice parameter and the lattice parameter of the newly formed phase decreases. The lattice parameter shrinkage slows down significantly at around 120–140 mAh g^{-1} Li extraction, coinciding well with both the slope change in the electrochemical charge curve and the depletion (146 mAh g^{-1}) of the Mn^{3+}/Mn^{4+} redox couple. Beyond this capacity a second redox mechanism, most probably due to the oxygen oxidization from O^{2-} to O$^-$, has to take over.

Upon discharge the lattice parameter increases with a slope that is between the two different slopes in the charge, which may suggest the simultaneous activation of both redox mechanisms mentioned above. At the end of discharge, the lattice parameter converges to a smaller value than in the pristine phase. This is in contrast to the layered Li-excess materials which increase in volume upon initial cycling, due to oxygen release and concomitant reduction of Mn^{4+} to Mn^{3+} upon

discharge of the densified material [15,16]. This may further support our argument that in LNMO the additional capacity is caused by an oxygen redox reaction rather than by oxygen release, as we further demonstrate below.

To further clarify how oxygen participates in the electrochemical reaction, four samples were examined by EELS measurements: pristine LNMO, LNMO charged to 145 mAh g^{-1}, LNMO after first charge to 4.8 V, and LNMO after first charge/discharge cycle at 55 °C (Fig. 4). In Mn L-edge spectra, the L$_3$ and L$_2$ absorptions are due to the transition from Mn 2p$^{3/2}$ to 3d$^{3/2}$ and 3d$^{5/2}$ and from Mn 2p$^{1/2}$ to 3d$^{3/2}$, respectively. Previous studies have shown that the L$_3$/L$_2$ ratio is inversely proportional to the valence of Mn [17,18]. Our results in the inset of Fig. 4 show that the valence of Mn is around 3 + in the pristine material, and is oxidized towards 4 + upon the first charge. It is worth noting that no further oxidation of Mn is observed from the L$_3$/L$_2$ ration beyond 145 mAh g^{-1} of Li extraction up to 4.8 V. After the first cycle, the Mn valence is only slightly reduced below 3 +. The pre-edge around 535 eV in the O EELS K-edge spectrum is caused by the transition of O 1s electrons to the unoccupied 2p orbitals, which is hybridized with the TM 3d orbitals. The significant increase of pre-edge intensity in the sample charged to 4.8 V shown in Fig. 4 indicates the increased contribution of the oxygen 2p hole, or oxygen oxidation [19–22]. This increase of pre-edge intensity is only observed beyond 145 mAh g^{-1} Li extraction, the maximum capacity provided by Mn redox couple, indicating that a substantial part of capacity is provided by oxygen oxidation. It should also be noticed that the shift of the pre-edge to lower energy is only observed beyond 145 mAh g^{-1}, consistent with the proposed oxidation of the O 2p state. After the first cycle, the O K-edge largely returns to the pristine state, which suggests a reversible O redox reaction in the first electrochemical cycle of LNMO. This is consistent with the changes in the O K-edge found by Yabuuchi et al. by soft X-ray absorption spectra in a compound with similar chemistry [13]. Although no clear oxygen reduction plateau is observed in the discharge profiles, our EELS results confirm the reversible oxygen reduction. These results are fundamentally different from layered Li-excess materials, where O$_2$ is irreversibly released in the first cycle, which leads to a cation-densified material which operates on average on lower valence states than the original material [18]. In contrast, the LNMO material operates reversibly by means of oxygen oxidation and reduction in the material. It remains
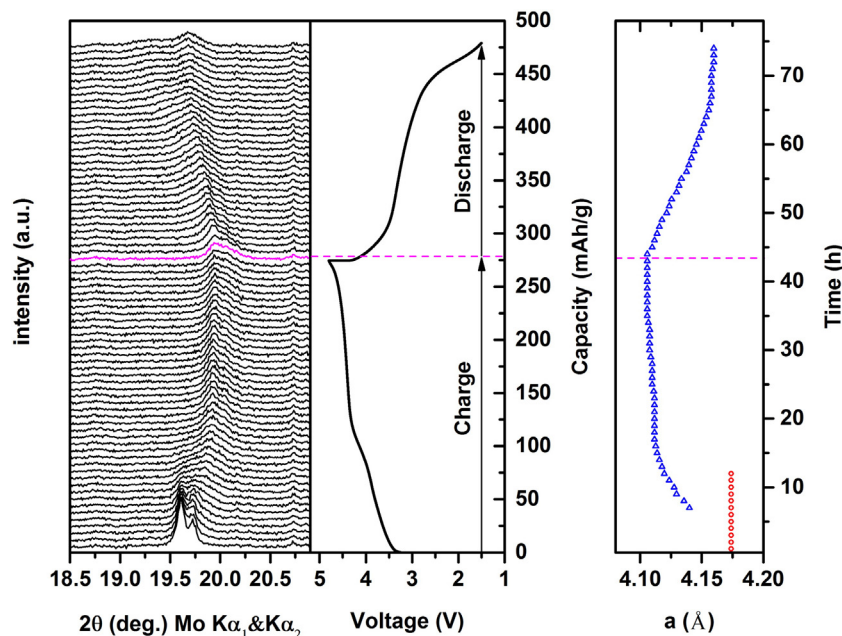

Fig. 3. In situ lab XRD taken at 1 h scanning rate per pattern shows the characteristic (200) peak evolution (left), corresponding to the in situ galvanostatic charge and discharge profiles (middle). The lattice parameter (right) is calculated from in situ XRD refinement. The double peaks are from the Kα1 and Kα2 emissions in the Mo X-ray source.
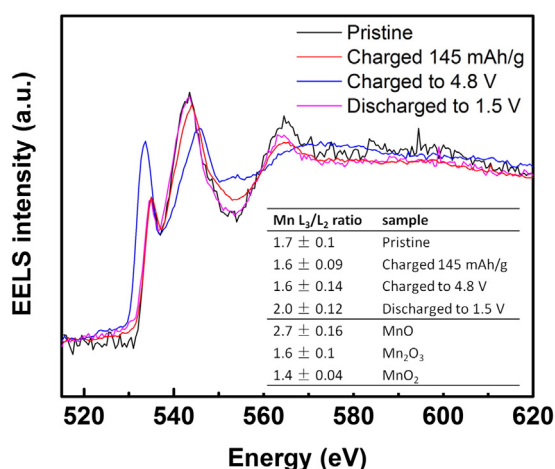
Fig. 4. EELS spectra of the O K-edge of LNMO at different charge states, aligned by Mn L_3/L_2 edges. Inset table shows the calculated L_3/L_2 ratio of Mn L_3/L_2 edges from different samples, where the values and standard deviations are averaged from 5 different measurements for each sample.

an open question how far such bulk oxygen oxidation can be pushed without decomposition of the material. The limit with no metal besides Li present at all is the Li-air system where a small amount of reversible Li de-intercalation from peroxide with concomitant oxidation of peroxide ions to superoxide ions was both theoretically predicted [23] and experimentally evidenced [24]. With the demonstration of reversible bulk oxygen oxidation through this work and several others, elucidating the minimal active and non-active metal content required in a Li-intercalation compound has become a fundamental and important challenge for the Li-ion battery field.

4. Conclusion

A disordered rock-salt material with Li-excess, $Li_{1.25}Nb_{0.25}Mn_{0.5}O_2$, has been synthesized and tested. It shows a high capacity of 287 mAh g^{-1} and specific energy density of 909 Wh kg^{-1} in the first cycle at 55 °C. Combined in situ XRD and EELS measurements indicate that Mn and O both reversibly contribute to the charge transfer with oxygen providing almost half of that capacity. Together with our previous work on understanding Li transport in Li-excess and disordered materials, we believe that this is an important new direction to create high capacity cathode materials.

Conflict of interest

There is no conflict of interest.

Acknowledgments

References

[1] M.M. Thackeray, C.S. Johnson, J.T. Vaughey, N. Li, S.A. Hackney, Advances in manganese-oxide 'composite' electrodes for lithium-ion batteries, J. Mater. Chem. 15 (2005) 2257–2267.

[2] Z. Lu, L.Y. Beaulieu, R.A. Donaberger, C.L. Thomas, J.R. Dahn, Synthesis, structure, and electrochemical behavior of Li[Ni$_x$Li$_{1/3 - 2x/3}$Mn$_{2/3 - x/3}$]O$_2$, J. Electrochem. Soc. 149 (2002) A778–A791.

[3] C.S. Johnson, J.S. Kim, C. Lefief, N. Li, J.T. Vaughey, M.M. Thackeray, The significance of the Li$_2$MnO$_3$ component in 'composite' xLi$_2$MnO$_3$ · (1 − x)LiMn$_{0.5}$Ni$_{0.5}$O$_2$ electrodes, Electrochem. Commun. 6 (2004) 1085–1091.

[4] R. Wang, X.Q. He, L.H. He, F.W. Wang, R.J. Xiao, L. Gu, H. Li, L.Q. Chen, Atomic structure of Li$_2$MnO$_3$ after partial delithiation and re-lithiation, Adv. Energy Mater. 3 (2013) 1358–1367.

[5] A. Ito, Y. Sato, T. Sanada, M. Hatano, H. Horie, Y. Ohsawa, In situ X-ray absorption spectroscopic study of Li-rich layered cathode material Li[Ni$_{0.17}$Li$_{0.2}$Co$_{0.07}$Mn$_{0.56}$]O$_2$, J. Power Sources 196 (2011) 6828–6834.

[6] B. Xu, C.R. Fell, M. Chi, Y.S. Meng, Identifying surface structural changes in layered Li-excess nickel manganese oxides in high voltage lithium ion batteries: a joint experimental and theoretical study, Energy Environ. Sci. 4 (2011) 2223–2233.

[7] N. Yabuuchi, K. Yoshii, S.T. Myung, I. Nakai, S. Komaba, Detailed studies of a high-capacity electrode material for rechargeable batteries, Li$_2$MnO$_3$–LiCo$_{1/3}$Ni$_{1/3}$Mn$_{1/3}$O$_2$, J. Am. Chem. Soc. 133 (2011) 4404–4419.

[8] M. Sathiya, G. Rousse, K. Ramesha, C.P. Laisa, H. Vezin, M.T. Sougrati, M.L. Doublet, D. Foix, D. Gonbeau, W. Walker, A.S. Prakash, M. Ben Hassine, L. Dupont, J.M. Tarascon, Nat. Mater. 12 (2013) 827–835.

[9] J. Lee, A. Urban, X. Li, D. Su, G. Hautier, G. Ceder, Unlocking the potential of cation-disordered oxides for rechargeable lithium batteries, Science 343 (2014) 519–522.

[10] V. Pralong, V. Gopal, V. Caignaert, V. Duffort, B. Raveau, Lithium-rich rock-salt-type vanadate as energy storage cathode: Li$_{2 − x}$VO$_3$, Chem. Mater. 24 (2012) 12–14.

[11] A. Urban, J. Lee, G. Ceder, The configurational space of rocksalt-type Oxides for high-capacity lithium battery electrodes, Adv. Energy Mater. 4: doi: 10.1002/aenm.201400478.

[12] R. Chen, S. Ren, M. Knapp, D. Wang, R. Witter, M. Fichtner, H. Hahn, Disordered lithium-rich oxyfluoride as a stable host for enhanced Li + intercalation storage, Adv. Energy Mater. 5: doi: 10.1002/aenm.201401814.

[13] N. Yabuuchi, M. Takeuchi, M. Nakayama, H. Shiiba, M. Ogawa, K. Nakayama, T. Ohta, D. Endo, T. Ozaki, T. Inamasu, K. Sato, S. Komaba, High-capacity electrode materials for rechargeable lithium batteries: Li$_3$NbO$_4$-based system with cation-disordered rocksalt structure, Proc. Natl. Acad. Sci. 112 (2015) 7650–7655.

[14] N. Twu, X. Li, A. Urban, M. Balasubramanian, J. Lee, L. Liu, G. Ceder, Designing new lithium-excess cathode materials from percolation theory: nanohighways in Li$_x$Ni$_{2 − 4x/3}$Sb$_{x/3}$O$_2$, Nano Lett. 15 (2015) 596–602.

[15] Z. Lu, J.R. Dahn, Understanding the anomalous capacity of Li/Li[Ni$_x$Li$_{(1/3 − 2x/3)}$Mn$_{(2/3 − x/3)}$]O$_2$ cells using in situ X-ray diffraction and electrochemical studies, J. Electrochem. Soc. 149 (2002) A815–A822.

[16] H.D. Liu, C.R. Fell, K. An, L. Cai, Y.S. Meng, In-situ neutron diffraction study of the xLi$_2$MnO$_3$ · (1 − x)LiMO$_2$ (x = 0, 0.5; M = Ni, Mn, Co) layered oxide compounds during electrochemical cycling, J. Power Sources 240 (2013) 772–778.

[17] X. Li, X. Ma, D. Su, L. Liu, R. Chisnell, S.P. Ong, H. Chen, A. Toumar, J.-C. Idrobo, Y. Lei, J. Bai, F. Wang, J.W. Lynn, Y.S. Lee, G. Ceder, Direct visualization of the Jahn–Teller effect coupled to Na ordering in Na$_{5/8}$MnO$_2$, Nat. Mater. 13 (2014) 586–592.

[18] C.R. Fell, D.N. Qian, K.J. Carroll, M.F. Chi, J.L. Jones, Y.S. Meng, Correlation between oxygen vacancy, microstrain, and cation distribution in lithium-excess layered oxides during the first electrochemical cycle, Chem. Mater. 25 (2013) 1621–1629.

[19] C.T. Chen, F. Sette, Y. Ma, M.S. Hybertsen, E.B. Stechel, W.M.C. Foulkes, M. Schluter, S.W. Cheong, A.S. Cooper, L.W. Rupp, B. Batlogg, Y.L. Soo, Z.H. Ming, A. Krol, Y.H. Kao, Electronic states in La$_{2 − x}$Sr$_x$CuO$_{4 + δ}$ probed by soft-x-ray absorption, Phys. Rev. Lett. 66 (1991) 104–107.

[20] W.S. Yoon, K.B. Kim, M.G. Kim, M.K. Lee, H.J. Shin, J.M. Lee, J.S. Lee, C.H. Yo, Oxygen contribution on Li-ion intercalation–deintercalation in LiCoO$_2$ investigated by O K-edge and Co L-edge X-ray absorption spectroscopy, J. Phys. Chem. B 106 (2002) 2526–2532.

[21] J. Graetz, C.C. Ahn, R. Yazami, B. Fultz, An electron energy-loss spectrometry study of charge compensation in LiNi$_{0.8}$Co$_{0.2}$O$_2$, J. Phys. Chem. B 107 (2003) 2887–2891.

[22] S. Miao, M. Kocher, P. Rez, B. Fultz, Y. Ozawa, R. Yazami, C.C. Ahn, Local electronic structure of layered Li$_x$Ni$_{0.5}$Mn$_{0.5}$O$_2$ and Li$_x$Ni$_{1/3}$Mn$_{1/3}$Co$_{1/3}$O$_2$, J. Phys. Chem. B 109 (2005) 23473–23479.

[23] S.Y. Kang, Y.F. Mo, S.P. Ong, G. Ceder, A facile mechanism for recharging Li$_2$O$_2$ in Li–O$_2$ batteries, Chem. Mater. 25 (2013) 3328–3336.

[24] K.P.C. Yao, Y.C. Lu, C.V. Amanchukwu, D.G. Kwabi, M. Risch, J.G. Zhou, A. Grimaud, P.T. Hammond, F. Barde, Y. Shao-Horn, The influence of transition metal oxides on the kinetics of Li$_2$O$_2$ oxidation in Li–O$_2$ batteries: high activity of chromium oxides, Phys. Chem. Chem. Phys. 16 (2014) 2297–2304.